Optimal alloying in hydrides: Reaching room-temperature superconductivity in LaH$_{10}$

Tianchun Wang [1,*] José A. Flores-Livas [2,3] Takuya Nomoto [4] Yanming Ma [5,6]
Takashi Koretsune [7] and Ryotaro Arita [3,4]

[1]*Department of Applied Physics, University of Tokyo, Tokyo 113-8656, Japan*
[2]*Dipartimento di Fisica, Università di Roma La Sapienza, Piazzale Aldo Moro 5, I-00185 Roma, Italy*
[3]*RIKEN Center for Emergent Matter Science, 2-1 Hirosawa, Wako 351-0198, Japan*
[4]*Research Center for Advanced Science and Technology, University of Tokyo, Meguro, Tokyo 153-8904, Japan*
[5]*State Key Laboratory of Superhard Materials, College of Physics, Jilin University, Changchun 130012, China*
[6]*International Center of Future Science, Jilin University, Changchun 130012, China*
[7]*Department of Physics, Tohoku University, Miyagi 980-8578, Japan*

Doping represents one of the most promising avenues for optimizing superconductors, such as high-pressure conventional superconductors with record-breaking critical temperatures. In this work, we perform an extensive search for substitutional dopants in LaH$_{10}$, looking for elements that enhance its electronic structure. In total, 70 elements were investigated as possible substitutions of La-sites at doping ratio of 12.5% under high pressure. To accelerate the screening of the ternary phases, our protocol to scan the chemical space is 1) to be constrained to highly symmetric patterns of hydrogen atoms, 2) focusing on phases with compact basis of lanthanum atoms (minimize enthalpy) and 3) to choose candidate dopants that preserve the van Hove singularity around the Fermi level. We found Ca as the best candidate dopants, which shift the van Hove singularity and increase the electronic DOS at the Fermi level. By using harmonic-level phonon calculations and performing first-principles calculation of T_c, Ca-doped LaH$_{10}$ shows T_c which is 15% higher than the one of LaH$_{10}$. It provides a promising route to reach room-temperature superconductivity in pressurized hydrides by doping.

I. INTRODUCTION

With the advent of hydrides as high-temperature superconductors, a particular emphasis has been put on studying pressurized hydrides systematically aided by computational methods. Using first-principles calculations, many efforts have been made to search for materials with higher transition temperatures and lower pressures [1–5]. With cooperations of theoretical prediction and experimental confirmation, pressurized hydrides led us to many important landmarks in superconductivity [1].

In general, high-pressure hydride superconductors can be classified to two classes structurally and chemically [1]. The first class includes H$_3$S [6,7] and PH$_3$ [8,9], in which covalent bond is predominantly present between hydrogen atom and sulfur or phosphorus atom. This covalent class of hydrides have a characteristic of relative low hydrogen ratio in their stoichiometries. This low hydrogen ratio is due to the bond saturation, with a reasonable maximum value of H$_5$. The second class is a more complex case featuring a strong covalent interaction between H$_2$ units. In this case hydrogen atoms form a network or clathrate, while the guest metal atom interacts with hydrogen in the range somewhere between ionic/covalent bond. Clathrate hydrides are a niche of hydride superconductors, and have a common denominator of high ratios of hydrogen, usually above H$_6$. The theoretical predictions of these superhydrides have been successfully

confirmed by experiments, among which notable reported cases are LaH$_{10}$ [10,11], YH$_6$ [12,13], YH$_9$ [13,14], and most recently an interesting case of CaH$_6$ [15,16].

In 2020, it was reported that carbonaceous sulfur hydride (CSH) was found to be a room-temperature superconductor (RTS) with a record-breaking transition temperature of $+15\,^\circ$C at 267 GPa [17,18]. Remarkably, the precise chemical composition and the crystalline form responsible for the RTS remain so far unclear. Theoretical studies have been carried out using different approximations and schemes [19–23], trying to figure out the atomic configuration responsible for the RTS. Considering the elements involved (C, S and H), we believe the recently reported CSH superconductor probably belongs to the covalent class. The discovery of CSH superconductor provides new sight for pressurized hydrides, however, further experimental evidence and confirmation are desperately required.

It is well understood that by introducing sufficient electron- or hole-donating impurities, semiconducting systems can be transformed into metallic phases. This strategy has been successfully demonstrated by inducing superconductivity in several semiconductors [24]. For instance, doped carbon allotropes are predicted to be superconductors at zero pressure [25–27]. Recent studies also point out the importance of hydrogenic bands to enhance T_c in known superconductors such as MgB$_2$ [28]. Similarly, the idea of doping under pressure has been used to predict that hydride clathrates systems such as H$_2$O [29] and polyethylene [30] will transform to metallic phases and display BCS superconductivity. Other studies focusing on hydrides also include the ternary

*tcwang@g.ecc.u-tokyo.ac.jp

C-S-H phase (guest-host $CH_4 + H_3S$ structure) [31,32] and doping in H_3S [20,33–35], revealing the potential to increase T_c of the parental phase H_3S. In addition, there have been predictions that some ternaries such as the electron-doped Li_2MgH_{16} [36,37] may show a T_c well above 300 K, though these systems may be elusive to synthesis [38] because of their complicated stoichiometry, pressure (> 2.5 Mbar), or other factors of stability.

Remarkably, doping has a potential to enhance T_c of hydride superconductors. From a theoretical perspective and a practical view, clathrate systems are the most promising ones for studying doping in hydride superconductors. The high hydrogen ratios ensure high T_c naively, and these systems have been proven to be thermodynamically stable down to pressure of 120 GPa. Compared to the covalent class, clathrate hydrides usually have high T_c above 240 K [10,11,39] under pressure as low as 150 GPa. This is a notable pressure difference of more than 110 GPa, compared to the pressure necessary to reach the room-temperature superconductivity at 267 GPa. Therefore, clathrate hydride systems are better candidates for us to study doping effect and find a route to higher T_c.

However, even for a modest ternary system, the computational overhead to pay for a thorough description of the phase diagram remains elevated. Here, we propose an alternative approach to accelerate the screening of ternary phases which is focusing only on the elements that can dope LaH_{10} under specific conditions. Based on the conclusions in Refs. [1,39], we propose following series of observations as a recipe guide or direction to screen for the best dopants in LaH_{10}: To maximize T_c in hydrides or other light-mass superconductors under pressure,

(1) It is best to have highly symmetric patterns of hydrogen configurations for hydride superconductors.

(2) A compact (dense) basis of lanthanum atoms (or guest atoms) that minimize the enthalpy is favorable.

(3) The electronic density of state should ideally display a van Hove singularity (VHS) at or close to the Fermi level.

(4) The heat of formation of the solid or the liquid metal alloy for the guest atoms should be favourable, i.e. the sought dopant atom should be miscible in the guest matrix, i.e., dopant atom X should be miscible to La, in the case of LaH_{10}.

In this work, we show that it is possible to enhance the electronic properties of LaH_{10} and induce a sizable change in the electronic occupation at the Fermi level while the electronic singularity is preserved. Using the computational and methodology presented in Sec. II, we will show the results on the structure stability of doped phases, electronic properties for best candidates, and the superconducting T_c for one of the candidates Ca-doped LaH_{10}.

II. COMPUTATIONAL DETAILS AND METHODOLOGY

Finding the best element that holds some of the above criteria can be accessed using first-principles calculations. To model doping we use supercells of the fcc ($Fm\overline{3}m$) of LaH_{10} at 150 GPa and substituted atoms in La sites. Originally, three doping-substitution percentages of 12.5%, 3.70% and 1.56% are studied. Considering the large computational cost of T_c calculation on supercells with low doping ratios and the trivial results of electronic DOS for 3.70% and 1.56% cases, we

only show the results of a thorough examination focusing on 12.5% doping ratio in this work, and we attach the results of structure studies and electronic structures for doping ratio of 3.70% and 1.56% to this work as Appendix A. The 12.5% doped case was simulated on the $2 \times 2 \times 2$ supercell with 8 formula units (f.u.) of LaH_{10} consisting of 88 atoms. Independent of chemical and logical reasons of substitutability, a total of 70 elements were tested (omitting 13 lanthanides, except for Lu). Total energy, enthalpy, atomic forces, and stresses are evaluated at the density functional theory (DFT) level with the Perdew-Burke-Ernzerhof Generalized Gradient Approximation (GGA-PBE) [40] parametrization to the exchange-correlation functional. We use a plane wave basis-set with the cutoff energy of 650 eV and the projector augmented wave (PAW) method [41] implemented in the Vienna *Ab Initio* Simulation Package (VASP) [42–45]. We use pseudopotential files POTCAR prepared for high pressure or with the highest number of valence electrons systematically for all elements. We used a tight criteria as atomic forces are less than two meV/Å and stresses are less than $0.01 \, eV/Å^3$ to control the convergence of our calculations. The electronic density of states (DOS) was integrated using the tetrahedron method for a single formula unit cell of LaH_{10} with 11 atoms, and a Γ-$44 \times 44 \times 44$ **k**-mesh (2,168 points in the irreducible part of the Brillouin zone (BZ)). For supercell calculations, we choose the Methfessel-Paxton sampling method [46] with dense $24 \times 24 \times 24$ **k**-meshes (Γ-centered, 413 points in the irreducible BZ) for supercell with 88 atoms.

Figure 1 shows the procedure applied to tackle the problem [1,47]. All the calculations of relaxation are performed at pressure of 150 GPa. A two-level geometry relaxation was carried out for the doped cases: the first one involved only volume optimization with fixed La atom basis, and the second one was studied with breaking symmetry of the doped La site. Different local relaxations were carried out per element per cell and calculations were accelerated using the GPU ported version of VASP [48]. In our calculations we find a positive correlation between the symmetry preserved in hydrogen cages and high DOS at the Fermi level. The occurrence of phase separation, broken H-cages or symmetrization from off-symmetry in relaxation results is relevant to predict whether electronic characteristics of candidates is trivial or not. Therefore, when phase separation to H_2, LaH_x and XH_x products occurs in the simulation, the DOS calculation will be skipped. However, if the geometry relaxation shows that the symmetry of H-cages is preserved and a high DOS at the Fermi level is observed in the calculation, the system will be accepted as a candidate and will be inspected for further studies.

To calculate T_c for candidate doped cases, we use the McMillan-Allen-Dynes (MAD) formula [49,50] as well as schemes based on the Migdal-Eliashberg (ME) theory [51,52]. The MAD formula is written as

$$T_c = \frac{\omega_{\log}}{1.2} \exp\left[\frac{-1.04(1+\lambda)}{\lambda - \mu^*(1 + 0.62\lambda)}\right], \quad (1)$$

with the electron-phonon coupling strength λ, the average phonon frequency $\omega_{\log}$, and the renormalized Coulomb parameter μ^*. The Migdal-Eliashberg calculation is done by
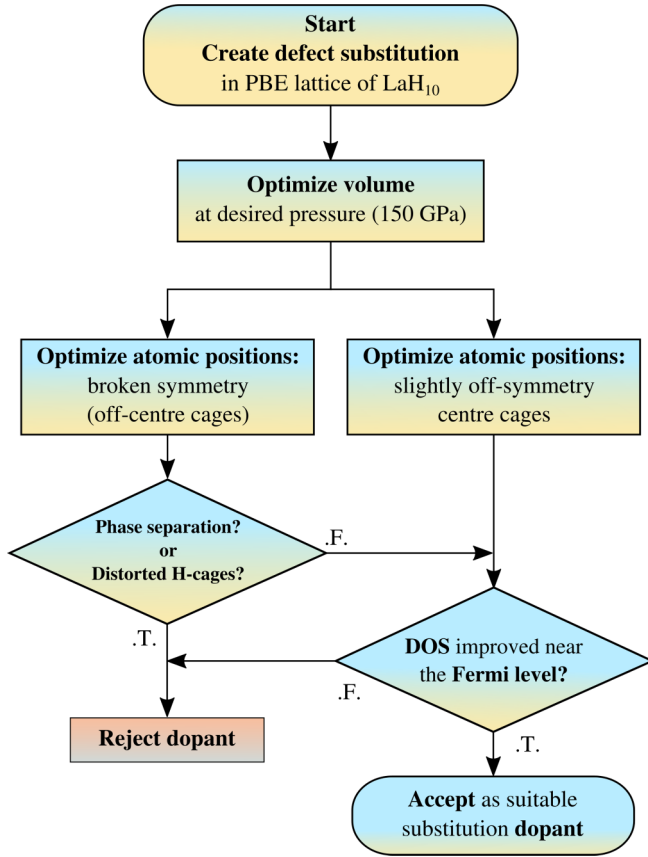
FIG. 1. Steps implemented in our computational study to search for suitable doping substitutions in LaH$_{10}$ under pressure.

solving the linearized gap equation as

$$\Delta_m(\boldsymbol{k}, i\omega_n) = -\frac{T}{N_{\boldsymbol{k}}} \sum_{m'} \sum_{\boldsymbol{k}', i\omega_{n'}} \mathcal{K}_{mm'}(\boldsymbol{k} - \boldsymbol{k}', i\omega_n - i\omega_{n'})$$
$$\times |G_{m'}(\boldsymbol{k}', i\omega_{n'})|^2 \Delta_{m'}(\boldsymbol{k}', i\omega_{n'}), \quad (2)$$

with the superconducting gap Δ, interaction kernel $\mathcal{K}$, and the dressed electronic Green's function G. Here $\boldsymbol{k}$ and $\boldsymbol{k}'$ denote the momentum of two pairing electronic states with band index m and m'. The Matsubara frequencies are written as $\omega_n = (2n+1)T$ for fermions and $\omega_\nu = 2\nu$ with integers n, ν, temperature T, and $N_{\boldsymbol{k}}$ is the total number of $\boldsymbol{k}$ points in the reciprocal space. The interaction kernel consists of contributions from the electron-phonon interaction and the RPA-type screened Coulomb interaction with static approximation. Details of the Green's functions and construction of interaction kernels can be found in Appendix B. This Migda-Eliashberg scheme and the approximations employed has been successfully used in other systems with conventional superconductivity [53,54]. We perform the DFT calculations and then the density functional perturbation theory (DFPT) calculations using QUANTUM ESPRESSO [55]. The parameter settings and pseudopotentials for the DFT calculation are the same as the ones used in the structure relaxations. Following the DFT calculations, the results of electronic energy spectrum, phonon frequency and the electron-phonon interaction

matrix element are used to perform the Migdal-Eliashberg calculation.

III. RESULTS AND DISCUSSIONS

A. Crystal structure and stability

In Fig. 2 we show a periodic tables containing elements considered as substitutions in La-matrix, and structures after relaxations of typical elements. Elements coloured in dark grey were not considered in this study due to their reduced availability or complex chemistry. Most of the elements with $4f$ valence electron were excluded except for lutetium. Interestingly, with doping ratio of 12.5%, only three elements (coloured in red) match ideally to the H-cages and leave them intact, thus a high symmetric pattern is preserved. All the 15 elements coloured in yellow induce distortions of H-cages. For comparison, these are sizable distortions as the ones in LaH$_{10}$ (monoclinic $C2$ phase in Ref. [39]) but preserve a guest-host clathrate chemistry. The 35 elements colored in light-blue and 17 dark-blue elements play in favour of phase separations. At the doping level of 12.5%, the analysis based on bonding, X-ray diffraction patterns and nearest-neighbours elucidate two levels of phase separation: the first one favours LaH$_x$ + XH$_x$ and the second one is a ternary phase separation of LaH$_x$ + XH$_x$ and H$_2$ units detached. We note that the methodology for classifying results includes both visual inspection on the X-ray diffraction patterns and examination on atomic distances given by the geometry relaxation results. The criteria used for the classification is strict, and lead us to the results that only He, Ca and Hf leave the structure unchanged and symmetry of H-cage preserved. In Fig. 3 we show the optimized volume for the doping ratio of 12.5%, as supplementary information to the our geometry relaxation calculation.

We have also explored a higher doping ratio of 25% for the entire set of elements. However, we noticed that the chemistry of the LaH$_{10}$ system change enormously at this doping ratio. Indeed, for many elements, new crystalline structures are found after a thorough geometry optimization. At higher doping of 25%, i.e. one atom substituted per four La atoms, enthalpy plays in favour of other more stable structures, making the study of the 25% doping ratio widely deviate from our initial assumptions. In order to warrant meaningful results at such a large percentage, it would be necessary to calculate the formation enthalpy, which will be cumbersome and computationally intractable with such vast decomposition channels. Based on the structural patterns and results from the high-throughput, we claim that our results are valid for small doping percentage, approximately below 12.5%, where the enthalpy of parental phase dominates. For 12.5% ratio only 3 elements preserve the high symmetry. In the following part we will examine the electronic features and prospects for the ensemble of these dopants.

B. Enhanced electronic DOS upon doping

Ideally, from the perspective of electronic structures, one should look for a dopant that increases the density of states at the Fermi level. In Fig. 4, we present the DOS of top doped cases found using the methodology described in Sec. II. At
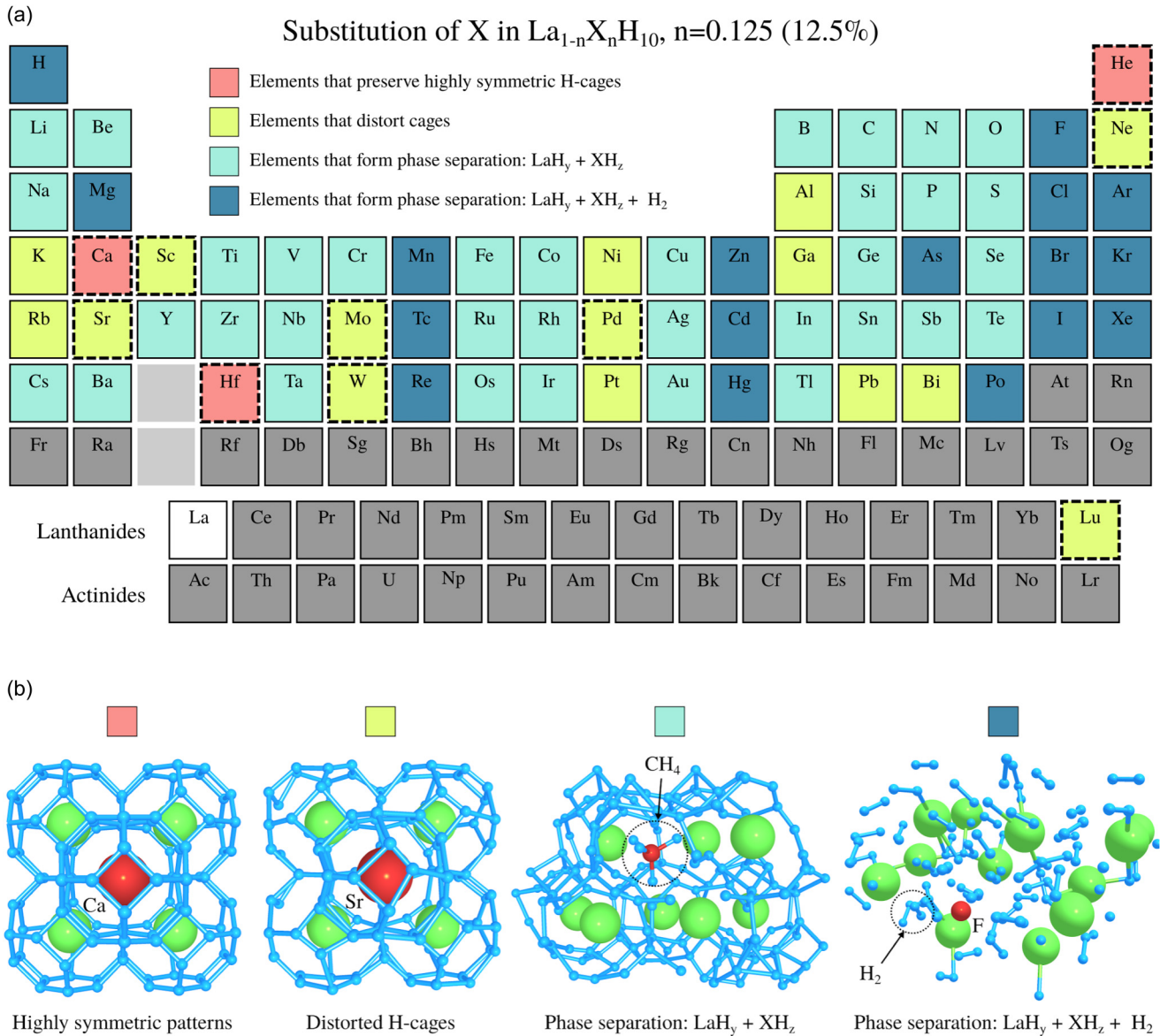
FIG. 2. Geometry relaxation results of LaH_{10} doped by different elements with doping ratio of 12.5% at 150 GPa pressure, and color code gives the behavior for different elements. (a) The periodic table with elements classified to four types of relaxation results. Dashed-squares are elements for which DOS is plotted in Fig. 4. Elements coloured in dark grey were not considered in this study. (b) Typical elements with corresponding structural patterns after relaxations for four cases. At the doping ratio of 12.5%, most of the elements destabilized the symmetric pattern, and only 3 elements preserve the high symmetry.

12.5% doping ratio, the most compelling cases are shown with solid lines (Ca, Hf and He) and the DOS of LaH_{10} is also shown as a reference. Overall, the shape of DOS is preserved in these cases. The Hf-doped case shifts the VHS to lower energies, and the Ca-doped case shows an interestingly result of bringing the VHS closer to the Fermi level.

Recently, Akashi [56] proposed a mechanism to explain the peaking of the DOS in a three-dimensional crystal and contrasted it for H_3S, which helps us to understand the formation of the VHS singularity in H_3S and LaH_{10}. At the pressure considered in this study (150 GPa), most of the doped elements greatly affect the electronic singularity. As is found in H_3S and LaH_{10} [39], the pressure dependence of the VHS is negligible. The *stability* of the VHS lies within a broad range. In the case of H_3S this range is from 120 GPa to 240 GPa. For LaH_{10}, the VHS appears around 110 GPa and extends beyond 300 GPa. These evidence hydrides' unique electronic features at high pressure.

It is clear that the crystalline structure of LaH_{10} and its electronic features [57] are pretty unique, and there is very little margin to improve it via doping. As is seen from Fig. 2, we can rule out following elements of Pt, Ga, Au, B, N, and C, which is contradictory to a recent work of a higher-order hydride suggested by Grockowiak *et al.* [58]. From our theoretical studies, these elements are highly reactive, not forming an ordered structure nor enhancing the DOS of LaH_{10}, at least in the doping ratio and pressure range studied in this work.

Furthermore, our results are in line with recent evidence found by Yi *et al.* [59], highlighting the importance of La atoms' metal framework for the excess electrons at interstitial
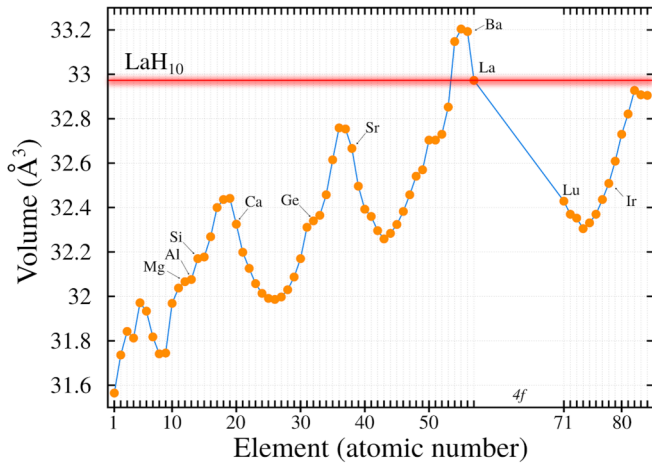
FIG. 3. Optimized volume for 12.5% doping ratio with different atoms at 150 GPa. Volume is optimized without breaking symmetry, thus the highly symmetric H-cages are preserved. Volume has been scaled to a single formula unit for comparison. Representative elements are marked as a guide, for which the DOS of these cases are plotted in Fig. 4. Red line represents the volume of the undoped case.

regions. Remarkably, the charge transfer from La to H atoms is mainly driven by the La framework's electride property. The interaction between La atoms and H cages induces the delocalization of La-$5p$ semi-core states to hybridize with H-$1s$ orbital. Thus, the bonding nature between La atoms and H cages is characterized as a mixture of ionic and covalent bond. Based on our results, we hypothesize that hydrides, when successfully synthesized at high pressure, are indeed very special and most of them will form quasi-perfect crystals. In the top panel of Fig. 5, we confirm that in LaH_{10} even a vacancy at a low concentration (one La atom missing for every $2 \times 2 \times 2$ supercell) will damages the VHS. This is in line with recent claims by Minkov *et al.* [60] for the case of D_3S, which shows a range of different T_c for different annealing paths [60]. Similarly, two different T_c onset exist in
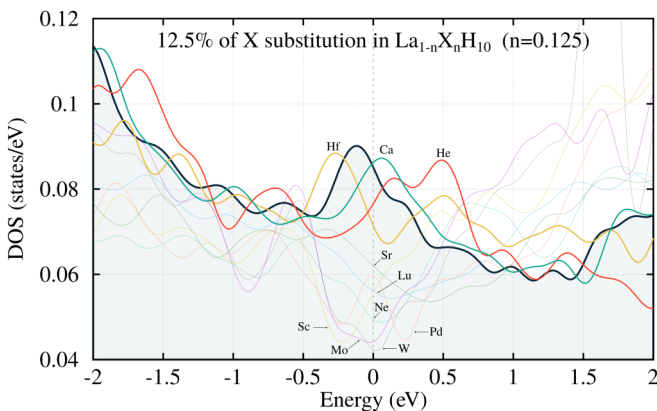

FIG. 4. Electronic density of states near the Fermi level for different doping atoms in LaH_{10} (fully optimized geometry at 150 GPa). Solid lines represent interesting dopants and lighter-dashed colors represent less relevant cases. For comparison, the DOS of LaH_{10} (pure phase) is shown in black-line (a grey area) calculated in the supercell.
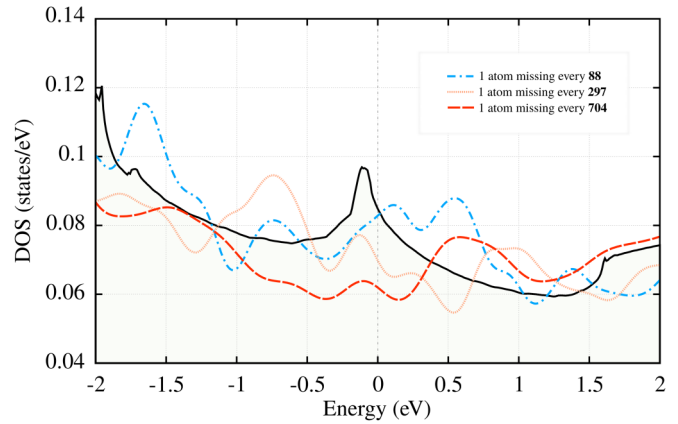

FIG. 5. Comparison of DOS for LaH_{10} and the case with a single vacancy in the La-site, for three different concentrations (one La atom missing for every $2 \times 2 \times 2$ supercell (88 atoms); one La atom missing for every $3 \times 3 \times 3$ supercell (297 atoms); one La atom missing for every $4 \times 4 \times 4$ supercell (704 atoms)).

LaH_{10} [11], which are above 260 K and close to 250 K with a dome-shape like behavior under pressure [10]. Presumably, in other systems such as yttrium hydride [12,13] and thorium hydride [61], deviations on the measured values of T_c seem to be correlated more with the annealing procedure and less with the H-content.

In the present study, we cannot rule out the possibility that a complete quantum treatment of nuclear positions symmetrizes some of the doped cases, while otherwise at the classical level it will be distorted. However, verifying this is not computationally tractable for simulating dopants through large supercells (hundreds of atoms per primitive cell). An indirect way to verify this effect has been discussed in Appendix C, as supplementary results of our attempt to solve this problem.

In the following discussions of T_c calculation, we neglect the quantum effect of atomic nuclei and stay in the classical level treatment. Following the results of structure relaxation in Fig. 2 and enhanced DOS in Fig. 4, we choose Ca-doped LaH_{10} as the best candidate, which brings the VHS closer to the Fermi level. This means Ca-doped case has potentially higher T_c than the one of LaH_{10}. In Sec. III C we move forward
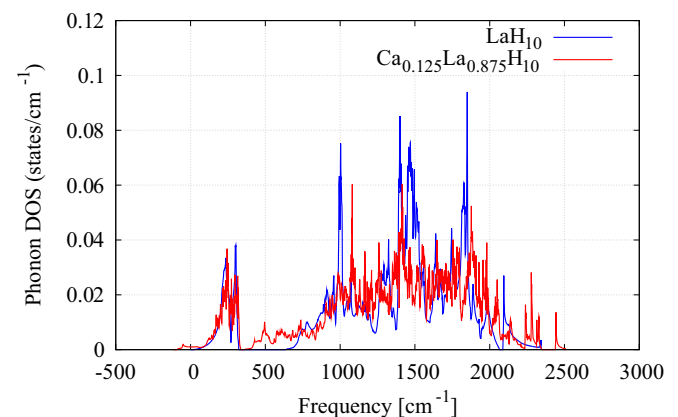

FIG. 6. The phonon DOS of LaH_{10} (blue) and Ca-doped LaH_{10} (red) with doping ratio of 12.5% at 300 GPa.
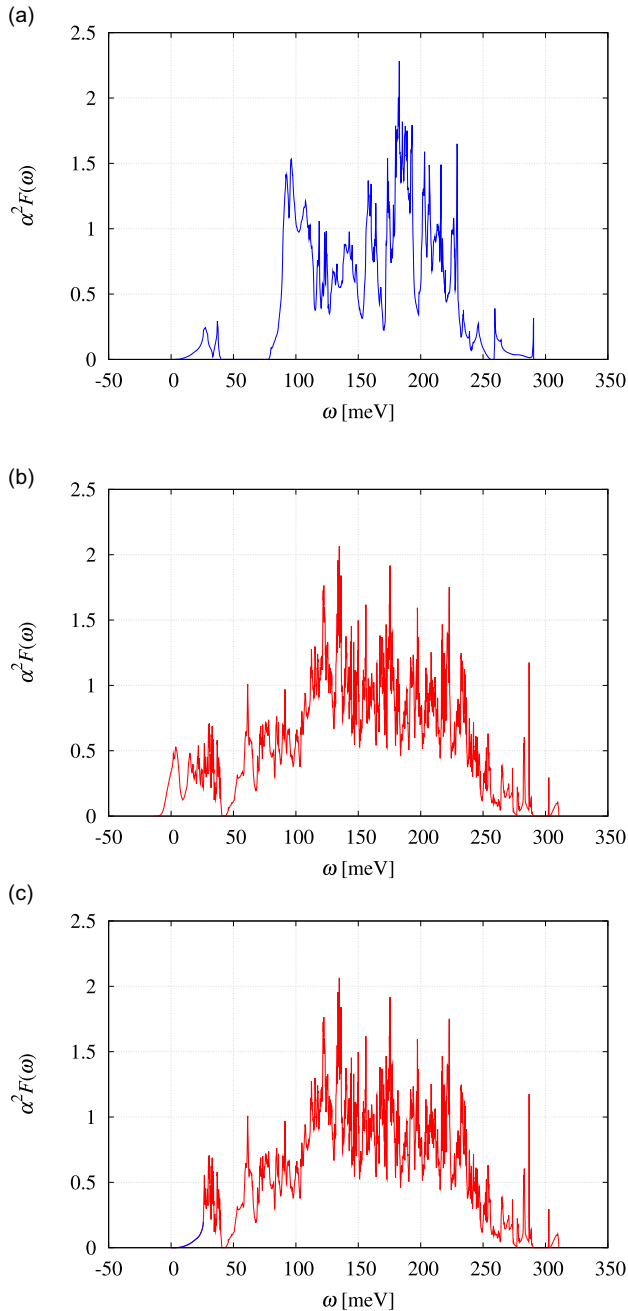
FIG. 7. The Eliashberg spectral functinon $\alpha^2 F(\omega)$ at 300 GPa for (a) LaH_{10} and (b) Ca-doped LaH_{10} with doping ratio of 12.5%. (c) The Eliashberg spectral function $\alpha^2 F(\omega)$ of Ca-doped LaH_{10} used in our practical calculation, in which the low frequency part $\omega < 15$ meV (blue) is from the one of (a) LaH_{10}, and the part of $\omega < 15$ meV (red) is the same as the one of (b) Ca-doped LaH_{10}.

C. Superconductivity of $Ca_x La_{1-x} H_{10}$ at 300 GPa

Considering the anharmonicity in the phonons of La-H systems [39] and limitations in our T_c calculation scheme to treat anharmonic phonons, we examine the superconductivity

of Ca-doped LaH_{10} at 300 GPa. At pressure of 300 GPa, the effect of anharmonicity can be neglected and harmonic phonons are sufficient for the T_c calculation. Since T_c of LaH_{10} has been shown to have monotonic dependence of pressure [39], calculations at 300 GPa can be a guide for us to examine the enhancement of T_c by doping Ca atoms. Following the results in Sec. III B, here we calculate the Ca-doped case with $x = 0.125$ using a $2 \times 2 \times 2$ supercell. We use a $6 \times 6 \times 6$ **k**-mesh and a $3 \times 3 \times 3$ **q**-mesh for the DFPT calculation, and we use a $12 \times 12 \times 12$ **k**-mesh for the calculation of the electron-phonon interaction as well as the Migdal-Eliashberg calculation.

In Fig. 6 we show the results of phonon DOS and in Fig. 7 we show the Eliashberg spectral function for 12.5% Ca-doped LaH_{10}. In the calculation of Ca-doped LaH_{10}, phonons with small negative frequency ~ 10 meV were discovered. With the assumption that this small negative modes are origimted from supercells are small and numerical errors in the calculation, we fix the low frequency part $\omega < 15$ meV of the Eliashberg spectral function $\alpha^2 F(\omega)$ by replacing this part with the one of LaH_{10}, as is shown in the bottom panel of Fig. 7. Then this $\alpha^2 F(\omega)$ is used in the following estimation of λ and $\omega_{\log}$. For the Migda-Eliashberg calculation negative value of phonon frequencies will be replaced by zero. The electron-phonon calculation shows that $Ca_x La_{1-x} H_{10}$ has strong electron-phonon coupling strength as LaH_{10}, with $\lambda = 2.8$ and $\omega_{\log} = 1163$ K. Using the MAD formula we have $T_c^{MAD} = 203.2$ K with $\mu^* = 0.1$, and as a reference for the case of LaH_{10} we obtain a result of 195.5 K. However, the the MAD formula Eq. (1) tends to underestimate T_c [50], especially in the strong electron-phonon coupling regime as in these systems. In such cases, the ME calculation will give a more accurate results of T_c. In practical ME calculations, we have added a parameter $\tilde{\lambda}$ at the left hand side of Eq. (2), and solve the equation as an
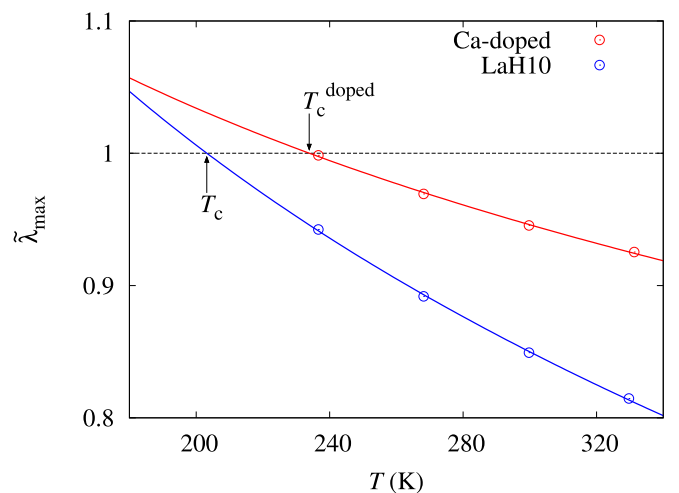

FIG. 8. Eigenvalue $\tilde{\lambda}_{\max}$ vs T in the Migdal-Eliashberg calculation. Red and blue circles represent the results of Ca-doped LaH_{10} and LaH_{10} respectively at 300 GPa. Solid lines are fitting results using fitting formula $\tilde{\lambda}_{\max} = A \log T + B$ via parameter A and B. Extrapolation of the fitting results shows $T_c = 203.2$ K for LaH_{10} and $T_c^{doped} = 233.9$ K for the doped case $Ca_x La_{1-x} H_{10}$.

to the electron-phonon interaction properties and predicted T_c for the case of Ca-doped LaH_{10}.

(a)

Substitution of X in La$_{1-n}$X$_n$H$_{10}$, n=0.0370 (3.70%)

(b)

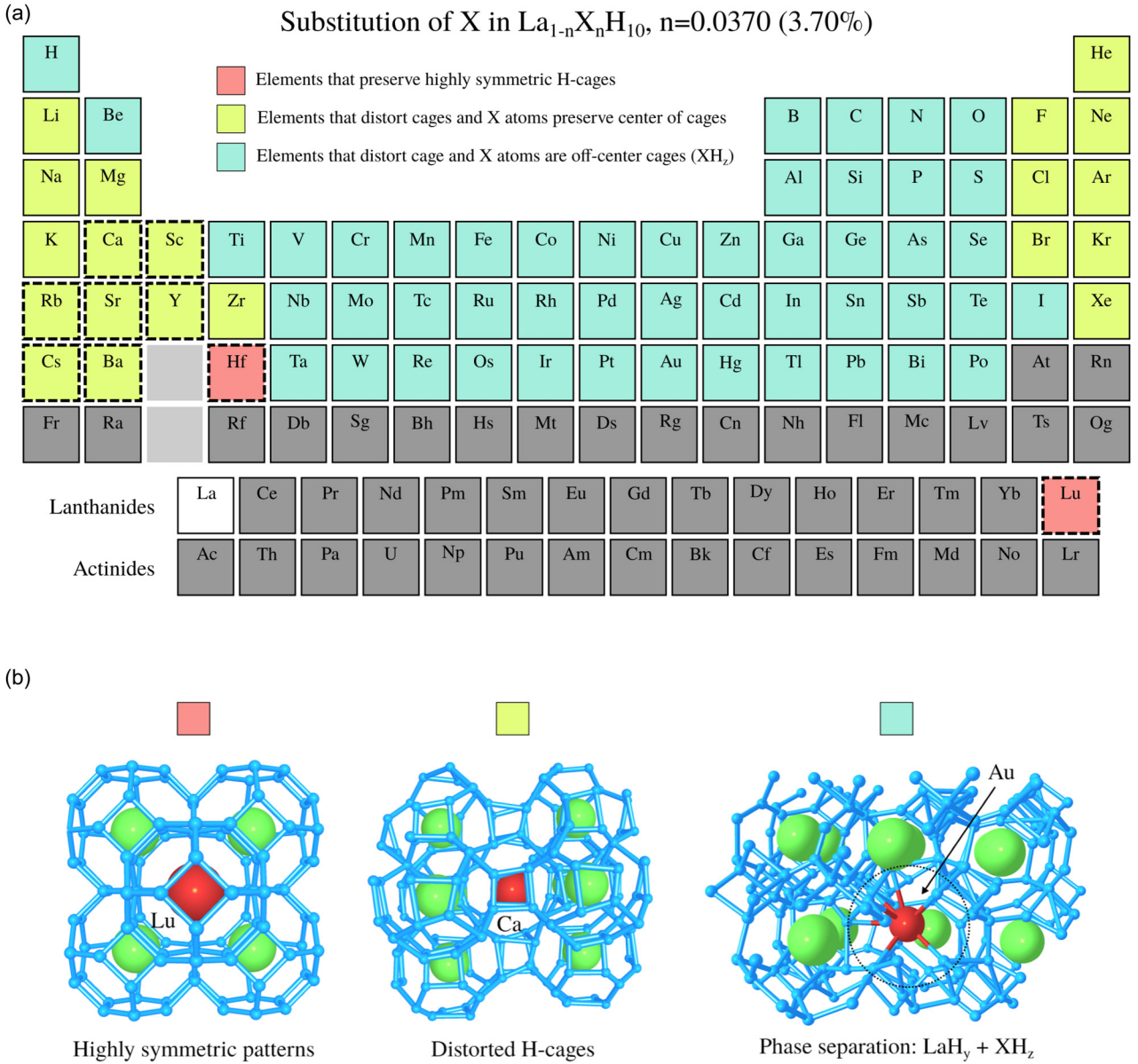| Highly symmetric patterns | Distorted H-cages | Phase separation: LaH$_y$ + XH$_z$ |

FIG. 9. Geometry relaxation results of LaH$_{10}$ doped by different elements with doping ratio of 3.70% at 150 GPa pressure, and color code gives the behavior for different elements. (a) The periodic table with elements classfied to three types of relaxation results. Dashed-squares are elements for which DOS is plotted in Fig. 12. Elements coloured in dark grey were not considered in this study. (b) Typical elements with corresponding structural patterns after relaxations for three cases. At the doping ratio of 3.70%, only 2 elements preserve the high symmetry.

eigenvalue problem

$$\tilde{\lambda}\Delta = \mathcal{A}\Delta, \tag{3}$$

in which $\mathcal{A}\Delta$ represents the right hand side of Eq. (2) including temperature T. The largest eigenvalue $\tilde{\lambda}_{max}$ reaches one when $T = T_c$. In Fig. 8 we compare the results of LaH$_{10}$ and Ca-doped LaH$_{10}$, with T_c enhanced by 30 K by doping. This enhancement of T_c is caused by the shift of the VHS, the increase of the DOS at the Fermi level, and therefore a stronger electron-phonon coupling, which agrees with our initial proposal. Based on previous experimental evidence of LaH$_{10}$ [10,11], with 15% enhancement of T_c in LaH$_{10}$ system, Ca doping provides us a promising route to reach room-temperature superconductivity at pressure $\lesssim$ 170 GPa [62].

IV. CONCLUSIONS

In conclusion, a thorough study of doping and structural stability for a wide variety of elements reveals the possibility to tune the electronic structure of LaH$_{10}$ under pressure. Among these elements, Ca-doping shows the potential to increase the DOS at the Fermi level and enhance T_c of LaH$_{10}$. Using first-principles Migdal-Eliashberg calculation, we show that T_c of Ca$_x$La$_{1-x}$H$_{10}$ is 15% higher than the one of LaH$_{10}$ with doping ratio $x = 12.5\%$. This provides us a promising route to reach room-temperature superconductivity at pressure in LaH$_{10}$ system at $\sim$ 150 to 170 GPa. Meanwhile, this process of screening based on structure relaxation and electronic structure calculation can be generalized to apply to
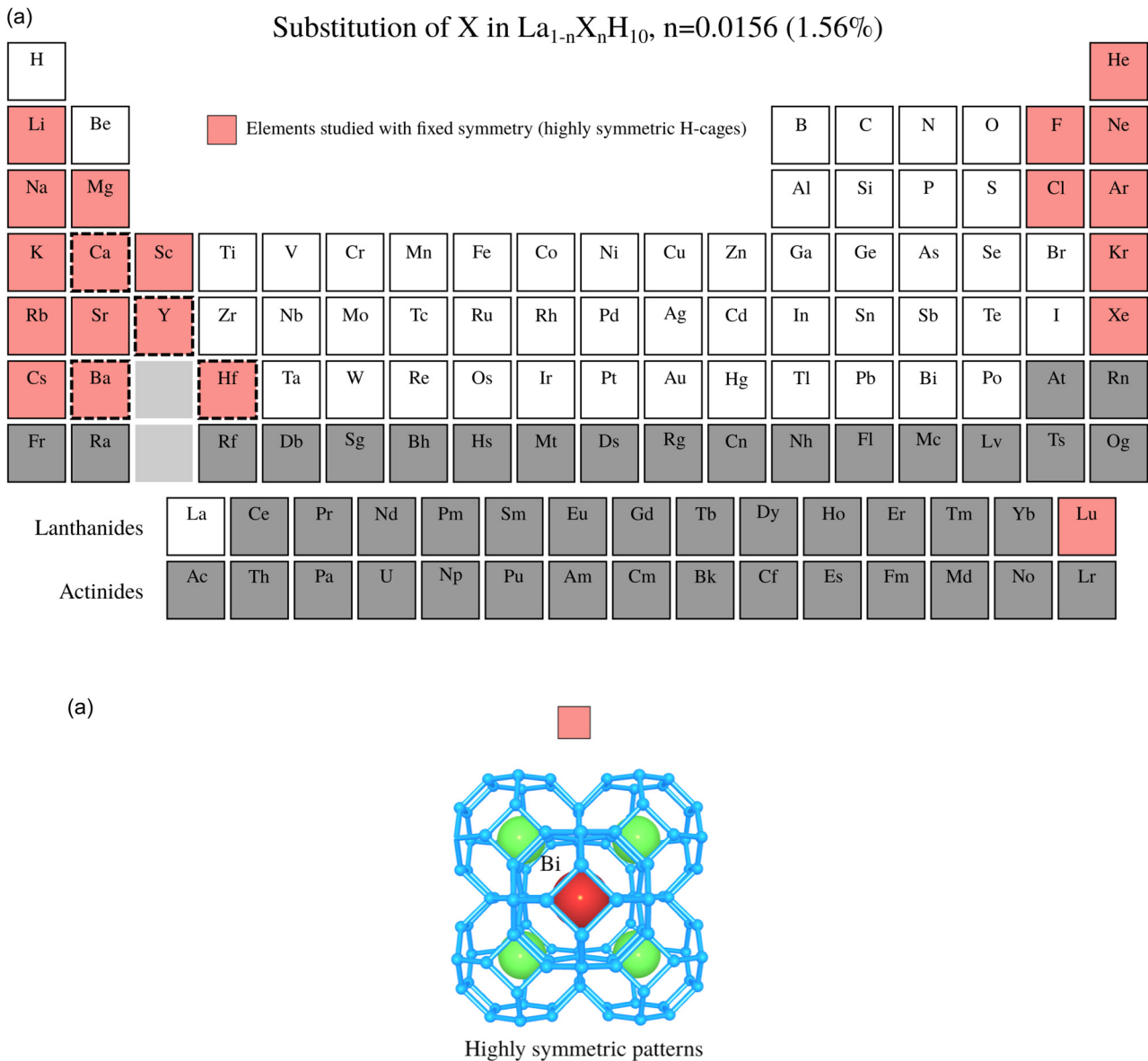
(a)

FIG. 10. Geometry relaxation results of LaH_{10} doped by different elements with doping ratio of 1.56% at 150 GPa pressure. (a) The periodic table with elements which show results with fixed symmetry (highly symmetric H-cages). Dashed squares are elements for which DOS is plotted in Fig. 12. Elements colored in dark grey were not considered in this study. Especially, Elements colored in white were not considered in this case of 1.56% doping ratio case. (b) Typical elements with corresponding structural patterns after relaxations. At low doping ratio of 1.56%, many elements preserve the H-cages.

other clathrate hydride systems to reach higher T_c by optimal doping.

APPENDIX A: RESULTS OF LOW DOPING RATIO OF 3.70% AND 1.56%

The 3.70% case is simulated using the $3 \times 3 \times 3$ supercell with 297 atoms (27 f.u.). For 1.56% case, we use 704 atoms and a $4 \times 4 \times 4$ supercell (64 f.u.). We use the Methfessel-Paxton sampling method with $16 \times 16 \times 16$ $\boldsymbol{k}$-mesh (145 points) for supercell with 297 atoms, and $10 \times 10 \times 10$ $\boldsymbol{k}$-mesh (47 points) for supercell with 704 atoms.

Figures 9 and 10 show the geometry relaxation results of doping ratio 3.70% and 1.56% respectively. In Fig. 11 we

(a)

Substitution of X in $La_{0.963}X_{0.037}H_{10}$ (3.70%)

(b)

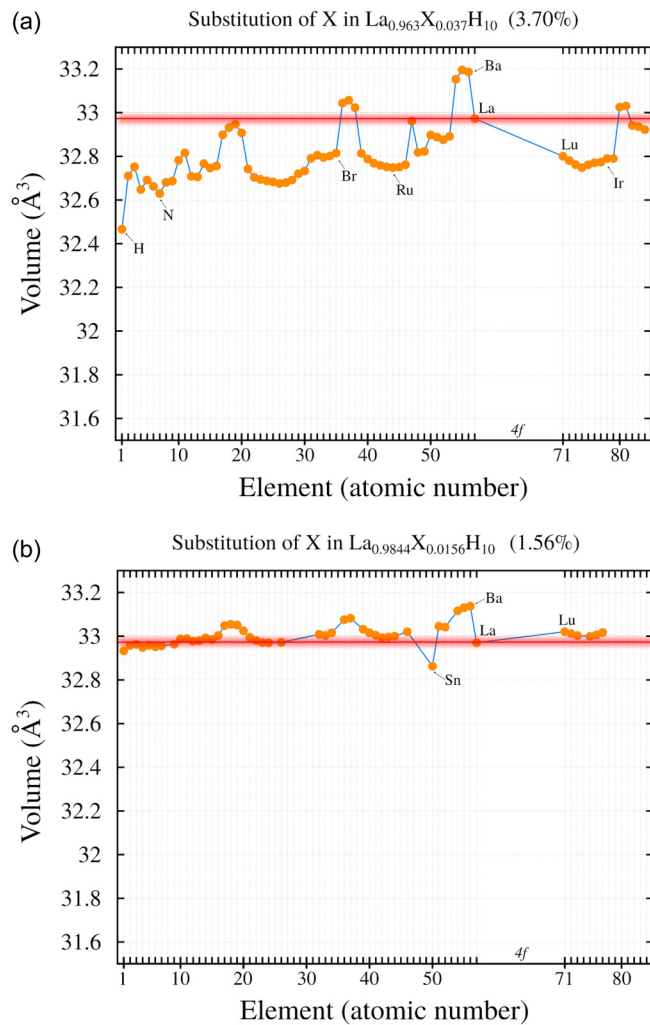**Substitution of X in $La_{0.9844}X_{0.0156}H_{10}$ (1.56%)**

FIG. 11. Optimized volume for (a) 3.70% and (b) 1.56% doping ratio with different atoms at 150 GPa. Volume is optimized without breaking symmetry, thus the highly symmetric H-cages are preserved. Volume has been scaled to a single formula unit for comparison. Representative elements are marked as a guide, for which the DOS of these cases are plotted in Fig. 12. Red line represents the volume of the undoped case.

(a)

3.70% of X substitution in $La_{1-n}X_nH_{10}$ (n=0.0370)

(b)

1.56% of X substitution in $La_{1-n}X_nH_{10}$ (n=0.0156)

FIG. 12. Electronic density of states near the Fermi level for different doping atoms in LaH10 (fully optimized geometry at 150GPa) with (a) 3.70% and (b) 1.56% doping ratio. For comparison, the DOS of LaH10 (pure phase) is shown in black-line (a grey area) calculated in the supercell.

show the results of optimized volume for lower doping ratio 3.70% and 1.56%. Fig. 12 shows electronic DOS for selected dopants with doping ratio of 3.70% and 1.56%.

For 3.70% doping, we find only two elements (coloured in red), Hf and Lu, in which after a complete optimization (starting with broken symmetry) the structures were relaxed back to the symmetric position, preserving the highly symmetrical pattern of H-cages. The elements coloured in yellow are mostly group I, group II, halogen and noble gas elements that retain symmetric centres of the fcc La basis but induce deformation of the H-cages. Elements in light blue are transition metals and p-block elements for which the dopant's local environment produces XH_x phase (dopant atom is off-centred of the fcc basis). Based on the results of 3.70%, we optimized the volume only for particular cases as input for 1.56%. All the elements coloured in red are elements considered at the center of cages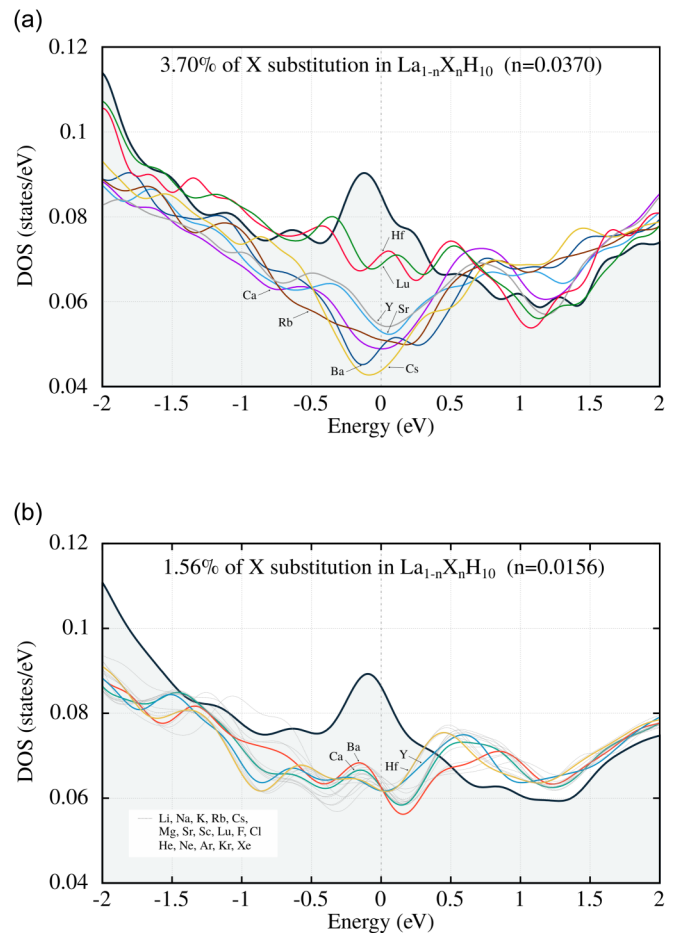 with highly symmetric hydrogenic cages (no broken symmetry). At doping ratio of 1.56%, alkali, alkaline-earth metals, halogens (Cl and F) and noble gases do not alter the initial patter of LaH_{10} at this pressure. From the structural point of view, all these elements are perfect candidates for doping, inducing small or no changes in the structure. In Fig. 10, white colored elements are not considered in our study of 1.56% doping ratio, since these elements have already shown distorted cage and off-center cage patterns in the study of 3.70% doping ratio.

According to Fig. 12, at 3.70% doping ratio Hf and Lu (the only elements that keep a highly symmetric structure) display DOS that are detrimental to the VHS. The rest of the elements ultimately removes the VHS. For the case of 1.56% doping, the elements that show relevant DOS are: Ba, Ca, Y, and Hf. However, it is noticeable that once the dopant is introduced, the volume change affects the charge transfer within the H-cage and the dopant. This volume change eventually reduces the singularity in these cases. It is shown that even low doping ratio of 3.70% induces sizable changes in the shape of DOS near the Fermi level. At the pressure considered in this study (150 GPa), most of the doped elements greatly affect the electronic singularity even at low limit ~1.56% doping.

APPENDIX B: DETAILS OF SUPERCONDUCTIVITY CALCULATION

In the McMillan-Allen-Dynes (MAD) formula, the electron-phonon coupling strength is

$$\lambda = 2 \int d\omega \frac{\alpha^2 F(\omega)}{\omega}, \tag{B1}$$

, and the average phonon frequency

$$\omega_{\log} = \exp\left[\frac{2}{\lambda} \int d\omega \frac{\alpha^2 F(\omega)}{\omega} \ln\omega\right], \tag{B2}$$

with the Eliashberg spectral function

$$\alpha^2 F(\omega) = \frac{1}{N(0)} \sum_{m\mathbf{k},m'\mathbf{k}'} \sum_{\gamma} |g_\gamma^{m\mathbf{k},m'\mathbf{k}'}|^2 \delta(\varepsilon_{m\mathbf{k}})\delta(\varepsilon_{m'\mathbf{k}'})$$

$$\times \delta(\omega - \omega_{\mathbf{q}\gamma}). \tag{B3}$$

For the Migdal-Eliashberg calculation, the interaction kernel consists of contributions from the electron-phonon interaction and the screened Coulomb interaction as

$$\mathcal{K}_{mm'}(\mathbf{q}, i\omega_\nu) = \mathcal{K}_{mm'}^{\text{el`}-\text{ph}}(\mathbf{q}, i\omega_\nu) + \mathcal{K}_{mm'}^{\text{C}}(\mathbf{q}, i\omega_\nu), \tag{B4}$$

where $\mathbf{q} = \mathbf{k} - \mathbf{k}'$ and

$$\mathcal{K}_{mm'}^{\text{el`}-\text{ph}}(\mathbf{q}, i\omega_\nu) = \sum_\gamma |g_\gamma^{mm'}(\mathbf{q})|^2 D_\gamma(\mathbf{q}, i\omega_\nu), \tag{B5}$$

$$\mathcal{K}_{mm'}^{\text{C}}(\mathbf{q}, i\omega_\nu) = \mathcal{K}_{mm'}^{\text{RPA}}(\mathbf{q}, i\omega_\nu = 0). \tag{B6}$$

For the electron-phonon interaction, $g_\gamma^{mm'}(\mathbf{q})$ is the $\mathbf{k}$-averaged electron-phonon interaction matrix elements, and the bare phonon Green's function is

$$D_\gamma(\mathbf{q}, i\omega_\nu) = -\frac{2\omega_{\mathbf{q}\gamma}}{\omega_\nu^2 + \omega_{\mathbf{q}\gamma}^2}, \tag{B7}$$

where $\omega_{\mathbf{q}\gamma}$ is the phonon frequency with mode index γ and the bosonic Matsubara frequency ω_ν. The screened Coulomb interaction kernel is an RPA-type kernel with static approximation $i\omega_\nu = 0$. The electronic Green's function evolved in Eq. (2) is the fully dressed one which satisfies the Dyson equation

$$G_m(\mathbf{k}, i\omega_n) = \frac{1}{i\omega_n - \varepsilon_{m\mathbf{k}} - \Sigma_m(\mathbf{k}, i\omega_n)}, \tag{B8}$$

and the electronic self-energy is written as

$$\Sigma_m(\mathbf{k}, i\omega_n) = -\frac{T}{N_\mathbf{k}} \sum_{m'} \sum_{\mathbf{k}', i\omega_{n'}} \mathcal{K}_{mm'}^{\text{el`}-\text{ph}}(\mathbf{k} - \mathbf{k}', i\omega_n - i\omega_{n'})$$

$$\times G_{m'}(\mathbf{k}', i\omega_{n'}). \tag{B9}$$

APPENDIX C: THE QUANTUM EFFECTS

Considering the quantum effects of nuclear positions and its effect on the results structure relaxation, here we indirectly verify it as we symmetrize the crystal structures (as observed in LaH_{10}) and map the variation of DOS and phonons dispersion. To examine any potential conflicts in our predictions originated from the lack of complete nuclear quantum treatment, we cross-check our results by imposing the symmetric structure, optimizing volume, and carefully checking the DOS
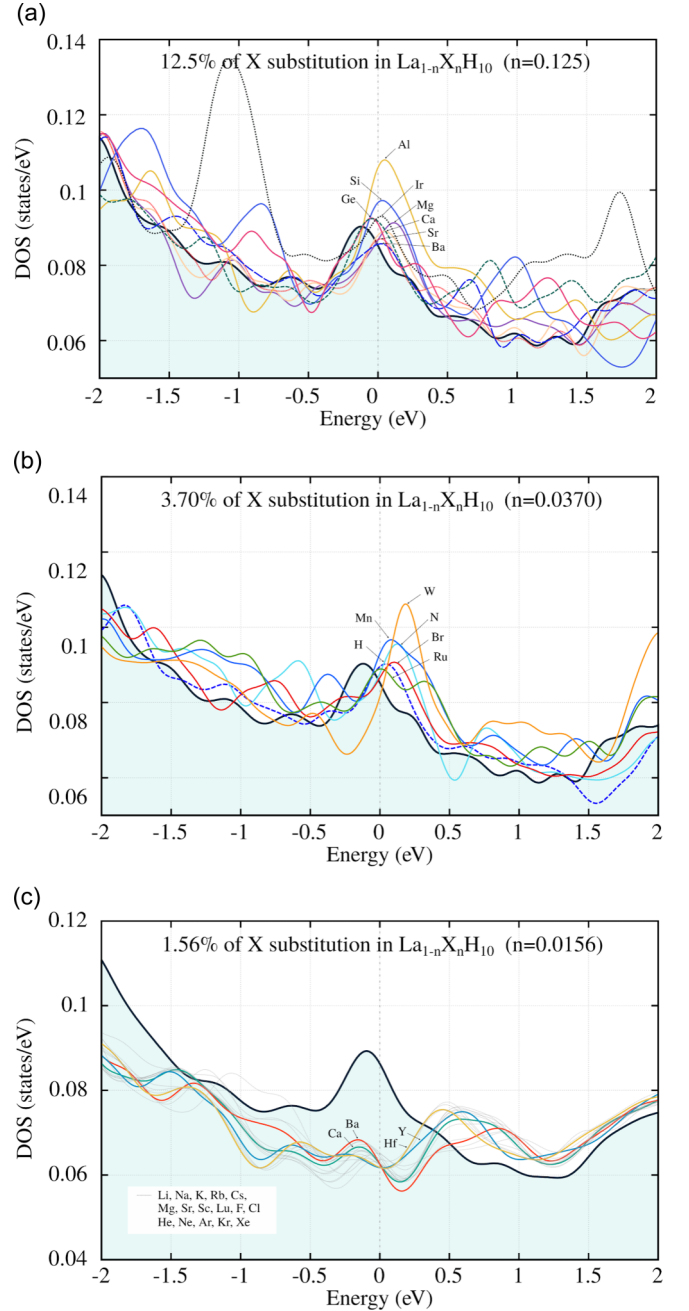

FIG. 13. DOS calculated for different dopants and different ratios of (a) 12.5%, (b) 3.70% and (c) 1.56% considering the quantum effects. Here we have assumed the symmetry of the fcc phase is preserved. The best elements for tuning the electronic structure in LaH_{10} at 150 GPa are Al, Si, Ge, Ir, Mg, Ca, Sr, and Ba at 12.5% doping ratio. For 3.7% doping ratio the best elements are Mn, N, Br, Ru, and H. In the case of even lower doping ratio, the incorporation of dopants, though in favor of thermodynamical stability, results in downturns of the stability of the van Hove singularity. In solid-line (in a grey area), the DOS of LaH_{10} for a single formula unit is shown.

for all doped cases with different percentages. Fig. 13 shows the elements that have a positive impact on the DOS when a highly symmetric pattern is preserved. Interestingly, Al, Si, Ir and H, donate the right amount of electrons to LaH_{10}, shift the VHS and increase the number of electrons at the Fermi

level substantially. If introduced in LaH_{10} at concentrations indicated, these elements could increase T_c to higher value. However, our calculations show that the Al-doped case is not stable under pressure of 250 to 300 GPa, and doping Al will finally result in the distortion of the H-cages. For the rest of the candidate dopants, it is possible that they can enhance the superconductivity in LaH_{10} considering the quantum effect, and further studies and examinations for these elements are required.

APPENDIX D: ENERGY OF MIXING

Considering the experimental synthesis process of Ca-doped LaH_{10}, here we give an estimation on the energy of mixing. The preparation of Ca-doped LaH_{10} can be regarded as a mixing process, and the Gibbs free energy of mixing is written as

$$\Delta G = \Delta H - T\Delta S, \tag{D1}$$

with the ideal entropy of mixing

$$\Delta S = R\left[x \ln x + (1-x)\ln(1-x)\right], \tag{D2}$$

where x is the doping ratio of Ca, and R is the ideal gas constant. The enthalpy of mixing is calculated as

$$\Delta H = H(Ca_xLa_{1-x}H_{10}) - xH(CaH_2) - 4xH(H_2)$$
$$- (1-x)H(LaH_{10}). \tag{D3}$$

At pressure of 300 GPa, the enthalpy of mixing obtained by our DFT calculation is $\Delta H = -3.46$ meV/atom, for which we take the $P6_3/mmc$ phase of CaH_2 and the $Cmca$ phase of H_2 into the calculation. In the case of $x = 0.125$ with temperature of $T = 300$ K, the entropy term is $T\Delta S = -9.74$ meV/atom. This result shows that the experimental synthesis of $Ca_xLa_{1-x}H_{10}$ will require a non-equilibrium structure preparation for $x = 0.125$, and a rough estimation shows that the equilibrium dopant concentration falls in $x < 0.05$.

[1] J. A. Flores-Livas, L. Boeri, A. Sanna, G. Profeta, R. Arita, and M. Eremets, Phys. Rep. **856**, 1 (2020).

[2] T. Bi, N. Zarifi, T. Terpstra, and E. Zurek, in *Reference Module in Chemistry, Molecular Sciences and Chemical Engineering* (Elsevier, Waltham, MA, 2019)

[3] C. J. Pickard, I. Errea, and M. I. Eremets, Annu. Rev. Condens. Matter Phys. **11**, 57 (2020).

[4] L. Zhang, Y. Wang, J. Lv, and Y. Ma, Nat. Rev. Mater. **2**, 17005 (2017).

[5] A. R. Oganov, C. J. Pickard, Q. Zhu, and R. J. Needs, Nat. Rev. Mater. **4**, 331 (2019).

[6] A. P. Drozdov, M. I. Eremets, I. A. Troyan, V. Ksenofontov, and S. I. Shylin, Nature (London) **525**, 73 (2015).

[7] M. Einaga, M. Sakata, T. Ishikawa, K. Shimizu, M. I. Eremets, A. P. Drozdov, I. A. Troyan, N. Hirao, and Y. Ohishi, Nat. Phys. **12**, 835 (2016).

[8] A. Drozdov, M. Eremets, and I. Troyan, arXiv preprint arXiv:1508.06224.

[9] J. A. Flores-Livas, M. Amsler, C. Heil, A. Sanna, L. Boeri, G. Profeta, C. Wolverton, S. Goedecker, and E. K. U. Gross, Phys. Rev. B **93**, 020508(R) (2016).

[10] A. Drozdov, P. Kong, V. Minkov, S. Besedin, M. Kuzovnikov, S. Mozaffari, L. Balicas, F. Balakirev, D. Graf, V. Prakapenka *et al.*, Nature (London) **569**, 528 (2019).

[11] M. Somayazulu, M. Ahart, A. K. Mishra, Z. M. Geballe, M. Baldini, Y. Meng, V. V. Struzhkin, and R. J. Hemley, Phys. Rev. Lett. **122**, 027001 (2019).

[12] I. A. Troyan, D. V. Semenok, A. G. Kvashnin, A. V. Sadakov, O. A. Sobolevskiy, V. M. Pudalov, A. G. Ivanova, V. B. Prakapenka, E. Greenberg, A. G. Gavriliuk, I. S. Lyubutin, V. V. Struzhkin, A. Bergara, I. Errea, R. Bianco, M. Calandra, F. Mauri, L. Monacelli, R. Akashi, and A. R. Oganov, Adv. Mater. **33**, 2006832 (2021).

[13] P. Kong, V. S. Minkov, M. A. Kuzovnikov, A. P. Drozdov, S. P. Besedin, S. Mozaffari, L. Balicas, F. F. Balakirev, V. B. Prakapenka, S. Chariton *et al.*, Nat. Commun. **12**, 5075 (2021).

[14] E. Snider, N. Dasenbrock-Gammon, R. McBride, X. Wang, N. Meyers, K. V. Lawler, E. Zurek, A. Salamat, and R. P. Dias, Phys. Rev. Lett. **126**, 117003 (2021).

[15] L. Ma, K. Wang, Y. Xie, X. Yang, Y. Wang, M. Zhou, H. Liu, X. Yu, Y. Zhao, H. Wang, G. Liu, and Y. Ma, Phys. Rev. Lett. **128**, 167001 (2022).

[16] Z. Li, X. He, C. Zhang, S. Zhang, S. Feng, X. Wang, R. Yu, and C. Jin, arXiv preprint arXiv:2103.16917.

[17] E. Snider, N. Dasenbrock-Gammon, R. McBride, M. Debessai, H. Vindana, K. Vencatasamy, K. V. Lawler, A. Salamat, and R. P. Dias, Nature (London) **586**, 373 (2020).

[18] R. P. Dias and A. Salamat, arXiv preprint arXiv:2111.15017.

[19] T. Wang, M. Hirayama, T. Nomoto, T. Koretsune, R. Arita, and J. A. Flores-Livas, Phys. Rev. B **104**, 064510 (2021).

[20] X. Wang, T. Bi, K. P. Hilleke, A. Lamichhane, R. J. Hemley, and E. Zurek, npj Comput. Mater. **8**, 87 (2022).

[21] M. Gubler, J. A. Flores-Livas, A. Kozhevnikov, and S. Goedecker, Phys. Rev. Materials **6**, 014801 (2022).

[22] Y. Ge, F. Zhang, R. P. Dias, R. J. Hemley, and Y. Yao, Materials Today Physics **15**, 100330 (2020).

[23] S. Hu, R. Paul, V. Karasiev, and R. Dias, arXiv preprint arXiv:2012.10259.

[24] E. Bustarret, Physica C: Superconductivity and its Applications **514**, 36 (2015).

[25] J.-Y. You, B. Gu, and G. Su, Phys. Rev. B **101**, 184521 (2020).

[26] C.-S. Lian, J.-T. Wang, W. Duan, and C. Chen, Sci. Rep. **7**, 1464 (2017).

[27] A. Sanna, A. Davydov, J. K. Dewhurst, S. Sharma, and J. A. Flores-Livas, Eur. Phys. J. B **91**, 177 (2018).

[28] J. Bekaert, M. Petrov, A. Aperis, P. M. Oppeneer, and M. V. Milosevic, Phys. Rev. Lett. **123**, 077001 (2019).

[29] J. A. Flores-Livas, A. Sanna, M. Graužinytė, A. Davydov, S. Goedecker, and M. A. Marques, Sci. Rep. **7**, 6825 (2017).

[30] J. A. Flores-Livas, M. Graužinytė, L. Boeri, G. Profeta, and A. Sanna, Eur. Phys. J. B **91**, 176 (2018).

[31] Y. Sun, Y. Tian, B. Jiang, X. Li, H. Li, T. Iitaka, X. Zhong, and Y. Xie, Phys. Rev. B **101**, 174102 (2020).

[32] W. Cui, T. Bi, J. Shi, Y. Li, H. Liu, E. Zurek, and R. J. Hemley, Phys. Rev. B **101**, 134504 (2020).

[33] C. Heil and L. Boeri, Phys. Rev. B **92**, 060508(R) (2015).

[34] Y. Ge, F. Zhang, and Y. Yao, Phys. Rev. B **93**, 224513 (2016).

[35] H. Guan, Y. Sun, and H. Liu, Phys. Rev. Research **3**, 043102 (2021).

[36] Y. Sun, J. Lv, Y. Xie, H. Liu, and Y. Ma, Phys. Rev. Lett. **123**, 097001 (2019).

[37] C. Wang, S. Yi, S. Liu, and J.-H. Cho, Phys. Rev. B **102**, 184509 (2020).

[38] J. A. Flores-Livas and R. Arita, Physics **12**, 96 (2019).

[39] I. Errea, F. Belli, L. Monacelli, A. Sanna, T. Koretsune, T. Tadano, R. Bianco, M. Calandra, R. Arita, F. Mauri, and J. A. Flores-Livas, Nature (London) **578**, 66 (2020).

[40] J. P. Perdew, K. Burke, and M. Ernzerhof, Phys. Rev. Lett. **77**, 3865 (1996).

[41] P. E. Blöchl, Phys. Rev. B **50**, 17953 (1994).

[42] G. Kresse and J. Hafner, Phys. Rev. B **47**, 558 (1993).

[43] G. Kresse and J. Hafner, Phys. Rev. B **49**, 14251 (1994).

[44] G. Kresse and J. Furthmüller, Comput. Mater. Sci. **6**, 15 (1996).

[45] G. Kresse and J. Furthmüller, Phys. Rev. B **54**, 11169 (1996).

[46] M. Methfessel and A. T. Paxton, Phys. Rev. B **40**, 3616 (1989).

[47] J. A. Flores-Livas, J. Phys.: Condens. Matter **32**, 294002 (2020).

[48] M. Hacene, A. Anciaux-Sedrakian, X. Rozanska, D. Klahr, T. Guignon, and P. Fleurat-Lessard, J. Comput. Chem. **33**, 2581 (2012).

[49] W. L. McMillan, Phys. Rev. **167**, 331 (1968).

[50] P. B. Allen and R. C. Dynes, Phys. Rev. B **12**, 905 (1975).

[51] A. Migdal, Sov. Phys. JETP **34**, 996 (1958).

[52] G. Eliashberg, Sov. Phys. JETP **11**, 696 (1960).

[53] W. Sano, T. Koretsune, T. Tadano, R. Akashi, and R. Arita, Phys. Rev. B **93**, 094525 (2016).

[54] T. Wang, T. Nomoto, Y. Nomura, H. Shinaoka, J. Otsuki, T. Koretsune, and R. Arita, Phys. Rev. B **102**, 134503 (2020).

[55] P. Giannozzi, O. Andreussi, T. Brumme, O. Bunau, M. B. Nardelli, M. Calandra, R. Car, C. Cavazzoni, D. Ceresoli, M. Cococcioni *et al.*, J. Phys.: Condens. Matter **29**, 465901 (2017).

[56] R. Akashi, Phys. Rev. B **101**, 075126 (2020).

[57] C. Wang, S. Yi, and J.-H. Cho, Phys. Rev. B **101**, 104506 (2020).

[58] A. D. Grockowiak, M. Ahart, T. Helm, W. A. Coniglio, R. Kumar, K. Glazyrin, G. Garbarino, Y. Meng, M. Oliff, V. Williams, N. W. Ashcroft, R. J. Hemley, M. Somayazulu, and S. W. Tozer, Frontiers in Electronic Materials **2**, 837651 (2022).

[59] S. Yi, C. Wang, H. Jeon, and J.-H. Cho, Phys. Rev. Materials **5**, 024801 (2021).

[60] V. S. Minkov, V. B. Prakapenka, E. Greenberg, and M. I. Eremets, Angew. Chem., Int. Ed. **59**, 18970 (2020).

[61] D. V. Semenok, A. G. Kvashnin, A. G. Ivanova, V. Svitlyk, V. Y. Fominski, A. V. Sadakov, O. A. Sobolevskiy, V. M. Pudalov, I. A. Troyan, and A. R. Oganov, Mater. Today **33**, 36 (2020).

[62] Regarding the experimental preparation of $Ca_xLa_{1-x}H_{10}$, we present an estimation of the energy of mixing and the equilibrium dopant concentration in Appendix D.